Supplementary Information
Programming stiff inflatable shells from planar patterned fabrics

Emmanuel Siéfert,[a] Etienne Reyssat,[a] José Bico,[a] Benoit Roman[a*]

[a]Laboratoire de Physique et Mécanique des Milieux Hétérogènes
CNRS, ESPCI Paris, Université PSL, Sorbonne Université, Université de Paris,
F-75005, Paris, France
* emmanuel.siefert@espci.fr.

Contents

Movies

Supplementary Movie 1
Manufacturing process of morphing fabrics structures.
Two heat-sealable sheets are superimposed and fixed in the working area of a CNC-machine. A heating head (soldering iron) is mounted on the machine and directly plots the desired welding pattern (video accelerated x80). The boundaries are then cut with scissors and a connector is inserted at the inlet of the structure. The structure is connected to a pressure supply (e.g. an inflating bulb) and buckles upon inflation into a 3D shape prescribed by the welding pattern.

Supplementary Movie 2
Anti-cone and saddle-shaped shells.
An archimedean spiral pattern (and thus nearly azimuthal welding direction) induces the radial contraction of the structure upon inflation, which buckles into an anti-cone. The structure has a diameter of 15 cm and is made of two superimposed Nylon fabric sheets (70den, one-sided TPU-coated, 170 g/sqm) from Extremtextil. Varying the relative welding width ξ in a nearly azimuthal channel pattern controls the local radial contraction rate λ, and a saddle of constant negative Gaussian Curvature may be programmed. The structure has a diameter of $25\,\mathrm{cm}$ and is made of two superimposed Ripstop-Nylon fabric sheets ($40\,$den, one-sided TPU-coated, $70\,\mathrm{g/m^2}$) from Extremtextil.

Supplementary Movie 3
Three different strategies to program a helicoid.
Three strategies may be used to distort the planar metric: changing only the orientation of the channels, playing additionally with the relative width of the seam lines, and making zigzag patterns of varying angle. Three helicoids are programmed using each method. The structures have a width of approximately $15\,\mathrm{cm}$ and are made of two superimposed Ripstop-Nylon fabric sheets ($40\,$den, one-sided TPU-coated, $70\,\mathrm{g/m^2}$) from Extremtextil.

Supplementary Movie 4
Influence of the zigzag angle χ on the principal contractions.
The variation of the angle χ of the zigzags induces a change in the ratio between the contraction along ($\lambda_{\|}$) and perpendicular ($\lambda_{\perp}$) to the averaged zigzag direction.

Supplementary Movie 5
Dome programmed with a zigzag pattern.
A dome of constant positive curvature can be programmed by varying the angle of zigzags (whose average direction is radial). The structure has a diameter of approx. $25\,\mathrm{cm}$ and is made of two superimposed Ripstop-Nylon fabric sheets ($40\,$den, one-sided TPU-coated, $70\,\mathrm{g/m^2}$) from Extremtextil.

Supplementary Movie 6
Gaussian shape programmed with a zigzag pattern.
The structure has a diameter of approx. $25\,\mathrm{cm}$ and is made of two superimposed Ripstop-Nylon fabric sheets (40 den, one-sided TPU-coated, $70\,\mathrm{g/m^2}$) from Extremtextil.

Supplementary Movie 7
Inflation of a 4 m wide structure, programmed to shape into a paraboloid.
The structure is made of two superimposed Nylon fabric sheets (70 den, one-sided TPU-coated, $170\,\mathrm{g/m^2}$) from Extremtextil. The welding pattern has been made using an ultrasonic sewing machine.

Supplementary Movie 8
Three layers structure.
Stacking three layers of fabric with specific welding patterns between the top-middle and middle-bottom layers enables to get two different shapes from one structure (when the top-middle pattern is inflated and when the middle-bottom one is inflated). Here, we reproduce the different shapes of the cap of algae *Acetabularia Acetabulum* during its growth [1].

Supplementary Movie 9
Hydrogel actuated structure
Two layers of standard cotton fabric can be simply sewed together along a specific pattern and small hydrogel beads ("water beads") can be inserted in the structure, which remains mostly flat. When immersed in water, the beads swell and deploy the structure into its target shape. The structure has a diameter of approx. $18\,\mathrm{cm}$. Total duration of the movie is one hour.

Structure fabrication

The fabrication of Gaussian morphing fabrics is relatively simple, since the manufacturing process is completely 2D.

Material Any thermoplastic material may be potentially used, including among others Mylar, polypropylene, polyethylene. Nevertheless, nylon textiles coated with thermoplastic urethane (TPU) matrix are best suited. They present the advantage to be easily and strongly sealed at relatively low temperature (around $150\,^{\circ}\mathrm{C}$). At such temperatures, only the TPU matrix melts and not the nylon textile, thus avoiding undesired puncture of the sheet while welding. Such fabrics are also stiff in the direction of nylon fibers (average Young's modulus of typically 1 GPa) while allowing some shear. This slight shear prevents the apparition of kinks and localized folds in the structure.

The structure is primarily made of two superimposed thermoplastic sheets that should be sealed together along a specific pattern. Various simple techniques may be used to weld the two sheets.

Heat printing A soldering iron may be mounted on an XY-plotter or a CNC-machine to directly "print" the heat-sealed seams pattern on the two superimposed sheets (Fig. 2a in the main document). We used the XY-plotter from Makeblock and a CNC Workbee from Openbuilds. The temperature, pressure and displacement velocity of the heating head are tuned in order to obtain a strong bonding between the two layers. These technical settings are however sensitive to the thickness and material properties of the sheets. The rationale behind the choice of parameters is the following: the temperature should be high enough to melt the TPU, the displacement velocity should be slow enough to ensure heat diffusion through the thickness of the sheet and the load applied on the tip should be high enough to impose a strong bonding (but too much loading may damage the sheets). In order to control the load at the tip, a slide is mounted on the Z axis of the plotter, the soldering iron being attached to the slide. Additional weights may be implemented to the slide to adjust the load. For the TPU-impregnated fabrics used in the illustrated examples, we set a typical speed of $150\,\text{mm/min}$, a total weight of approximately $500\,\text{g}$ and a head temperature at $220\,^{\circ}\text{C}$. The diameter of the head is around $1\,\text{mm}$.

If the sheet is coated on both sides with thermoplastic material, a sheet of baking paper is placed on top of the structure during the welding in order to protect the structure and to avoid the adhesion of the melted material on the printing head.

Heat press Alternatively, the pattern of air channels may be laser cut in baking paper so that the designed seam lines are cut out from the baking paper sheet. The resulting pattern is then placed between both thermoplastic fabric sheets; the whole sandwich is heat-pressed between two additional baking paper sheets to prevent the adhesion of melted thermoplastic on the heat press. The two fabric sheets are sealed together only where the baking paper has been cut out. The patterned baking paper remains trapped in the structure but does not play any mechanical role upon inflation.

Heat press mould This method is best suited for serial production of the same structure. A metallic plate is engraved except at the target location of the seam lines. It serves as a waffle iron in the heat press, welding only the appropriate lines on the surface. This fabrication technique could be directly used for industrial applications, enabling a large and cost-efficient throughput.

Other methods Alternatively, regular sewing is also possible to manufacture the structures, if a sealant film is applied on the seam lines to ensure air tightness. Any impermeable fabric may thus be used with such a fabrication strategy. Pressure within the structure may be caused by other means, including hydrogel beads swelling in water. In such a case, the fabric sheets have to be permeable to allow water diffusion in the structure, promoting the shape change (Supplementary movie 9).

Metric distortion strategies

1 Width of the seam

In the first presented version of these Gaussian morphing structures, inflated shapes only result from the local direction of the seam lines. An additional degree of freedom in the distortion of the flat metrics widens the possibilities of shape programming. A simple solution is to play with the relative seam width ξ to tune the homogenized in-plane contraction perpendicular to the seam direction (see Eq. 1 in the main manuscript).

Hemisphere. Consider purely radial airways, that induce azimuthal contraction. We define as u the curvilinear coordinate in the inflated structure and r the radial coordinate of the initially flat state. In the case of radial seams, there is no contraction in the radial direction ($u = r$). In order to program a portion of a sphere of radius R, the evolution of the azimuthal contraction λ_θ should follow:

$$\lambda_\theta(r) = \frac{R}{r}\sin\frac{r}{R} = 1 - \frac{r^2}{6R^2} + o((r/R)^2) \tag{1}$$

The relative seam width $\xi(r)$, may be easily computed by combining this relation with Eq. 1 from the main manuscript. The maximum achievable contraction is $2/\pi$, which enables us to program a hemisphere out of a flat disk (the equator indeed verifies $r/R = \pi/2$). The structure does buckle, when inflated, into a bowl shape that is close to the targeted hemisphere (Fig. 3f in the main manuscript). Nevertheless, the structure remains very floppy, as it may be easily folded along any radial seam.

Saddle. In order to program a saddle of constant negative Gaussian curvature K, the perimeters should bear excess length: $P(u) = 2\pi u(1 - Ku^2/6 + o(u^2))$. In the ideal case of purely azimuthal seams, perimeters remain unchanged upon activation, but the radii contract. At second order in r, the contraction should thus reads:

$$\lambda_r(r) = 1 + \frac{Kr^2}{6} \tag{2}$$

Although the weld lines are not perfectly azimuthal (spiral pattern), the obtained shape is satisfactory (Fig. 3g in the main manuscript) and appears to be stiff because of the curved seams.

Helicoid. Consider parallel seams of varying width. The contraction should be maximal at the center line of the ribbon and can be chosen as $\pi/2$ with no contraction along the edges.Thus, the maximum admissible ratio l/p, where l is the width of the ribbon and p the pitch of the helicoid, reads:

$$\frac{l}{p} = \frac{1}{2}\sqrt{\frac{\lambda_{max}^{-2} - 1}{4\pi^2}} \tag{3}$$

where λ_{max} corresponds to the maximum contraction, *i.e.* the minimal value of λ (λ_{max} is bounded by $2/\pi$ in the limit of vanishing thickness of the seam line). The variation of the targeted contraction rate $\lambda_\perp$ as a function of the coordinate along the seam $x_\parallel$ (the origin being chosen at the center of the ribbon) can be expressed as:

$$\lambda_\perp(x_\parallel) = \lambda_{max}\sqrt{1 + 4\pi x_\parallel^2/p^2} \tag{4}$$

Using equation (1) from the main article, the relative width of the seam ξ reads:

$$\xi(x_\parallel) = (\sqrt{1 + 4\pi x_\parallel^2/p^2} - 1)/(\lambda_{max}^{-1} - 1) \tag{5}$$

Additionally, two parallel stripes are sealed along the outer edges of the ribbon to ensure bending stiffness along the helicoid direction (Fig. 3h in the main manuscript).

The dome obtained with this strategy is very floppy, whereas the helicoid and the saddle are relatively stiff. Both structures indeed present a boundary that is not contracted along its tangent: the contraction is perpendicular to the boundary, which is stiffened by the presence of the curved air beam. This is possible only for negative curvatures, since the plate may only contract (and not extend) within a fixed boundary length. Another condition to obtain a stiff structure is to ensure that the welded portions are under tension. As they are very slender, they would indeed buckle for minute compressive forces.

2 Programming axisymmetric shapes with zigzag patterns

Using zigzag patterns (see main manuscript), simple geometric surfaces with Gaussian curvature may be programmed. Consider a target axisymmetric shape obtained by the revolution of the curve $z = f(\rho)$, where (ρ, z) correspond to the cylindrical coordinates. We consider zigzag patterns in the radial direction. In this case, the remaining degree of freedom is the internal zigzag angle $\chi(r)$, where r is the radial coordinate in the initially flat disk. Starting at the center of the disk ($r = 0$), the inflated structure should be locally flat to avoid a singular point, which imposes $\lambda_\perp = \lambda_\parallel$ and thus $\chi(r = 0) = 1/\sqrt{1 + \lambda}$. Making an infinitesimal step $\mathrm{d}r$ on the flat disk thus results in an infinitesimal step:

$$\mathrm{d}u = \lambda_\parallel(r)\mathrm{d}r \tag{6}$$

on the inflated curved surface. At this location, the needed azimuthal contraction simply reads:

$$\lambda_\perp = \rho/r \tag{7}$$

from which we retrieve the appropriate local angle $\chi(r)$. The infinitesimal step for ρ is set by the geometric relation:

$$\mathrm{d}u = \sqrt{\mathrm{d}\rho^2 + \mathrm{d}z^2} = \sqrt{1 + f'(\rho)^2}\,\mathrm{d}\rho \tag{8}$$

Putting the last three equations together and using the constant area contraction $\lambda_\perp \lambda_\parallel = \lambda$, we retrieve the following expression:

$$\lambda r \mathrm{d}r = \sqrt{1 + f'(\rho)^2}\,\rho \mathrm{d}\rho \tag{9}$$

The local angle $\chi(r)$ of radial zigzags follows the same evolution as the seam line orientation angle $\alpha(r)$ in spiral patterns [2].
Depending on the configurations, Eq. 9 may be solved analytically or numerically. A paraboloid is shown in Fig. 3j and Fig. 4 from the main manuscript. The shape of the inflated shell quantitatively matches the target profile (in red dashed lines). A Gaussian profile is presented in Fig. 3k from the main manuscript. This target shape is in practice not reachable with the strategy implying the variation of the width of the welded line. The curvature of the profile indeed induces compressive azimuthal forces, which would result in the buckling of the welded portions.

Structural Stiffness

In this section, we describe the stretching and bending stiffness and maximum admissible moment of straight inflated textile beams and arrays of zigzag beams, in order to better understand the mechanics of the structures we build.

1 Stiffness of straight lines

Consider a pair of facing strips of thickness t sealed along their edges of length l and width w, with $t \ll w \ll l$. The width of an assembly of N parallel inflated strips is thus $L_0 = 2Nw/\pi$. We define as $w^* = w - e$, the width of the unsealed portion of the fabric (in practice $e \ll w$). Upon inflation, the structure deforms into an air beam of circular cross section with radius $r = w/\pi$ if the pressure is large when compared with the bending resistance of the strips, i.e. if $p \gg Et^3/w^{*3}$, where E is the Young modulus of the fabric, which is the case in our experiments. We also assume that the stretching strain induced by pressure is small, i.e. $p \ll Et/w$, which is also verified experimentally.

Stretching. Along the beams, the stretching modulus of the inflated structure $Y_\parallel$ simply reads $Y_\parallel = \pi E t$ (the potential contribution from pressure scales as pw which is order of magnitudes smaller than stretching the sheet). Conversely, stretching the structure in the direction perpendicular to the seams means elongating the cross-section towards a solution that does not maximize the volume. Laplace law imposes the cross sections of the beams to remain portions

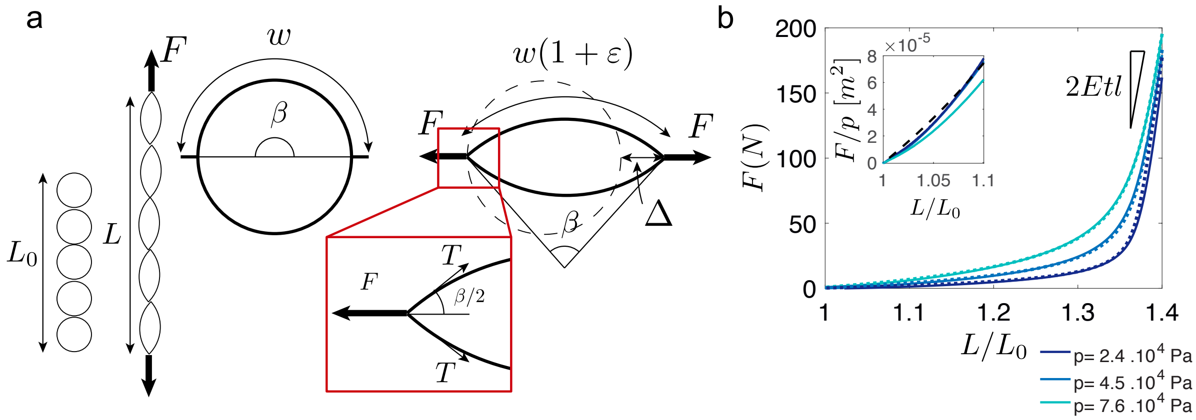

Figure 1: Stretching of the structure perpendicular to the direction of the seam. (a) Schematic cross section of an inflated beam at rest and under traction, with the spanned angle β, the effective strain at the scale of the sheet ε, the net displacement Δ and a zoom on the force balance at the seam. (b) Force-displacement curve for various pressures, with experimental measurements in solid lines, and theoretical prediction in dashed lines. Inset: rescaled force-displacement curve in the quasi-inextensible regime: the force does not depend on the properties of the sheet. The structure corresponds to 10 tubes with $w = 5.5\,\text{mm}$, $e = 1.7\,\text{mm}$, $E = 4.5.10^8$ Pa, and $t = 0.1\,\text{mm}$.

of circles of spanned angle β and corresponding radius of curvature $R = w^*(1+\varepsilon)/\beta$ (Fig. 1a), where ε is the (uniform) strain applied to the structure. The tension T in the sheet reads:

$$T = Et\varepsilon = pw^*(1+\varepsilon)/\beta \tag{10}$$

A simple force balance (Fig. 1a) gives the following expression for the force F (per unit length):

$$F = 2T\cos(\beta/2) \tag{11}$$

The corresponding total displacement Δ reads:

$$\Delta = L - L_0 = 2w^* \left((1+\varepsilon)\frac{\sin(\beta/2)}{\beta} - \frac{1}{\pi} \right) \tag{12}$$

Combining equations (10-12), one may eliminate T and ε, and express both the force and the displacement as a function of β

$$F = 2pw^* \frac{cos(\beta/2)}{\beta - \Sigma} \tag{13}$$

$$\Delta = 2w^* \left(\frac{\sin(\beta/2)}{\beta - \Sigma} - \frac{1}{\pi - \Sigma} \right) \tag{14}$$

where $\Sigma = pw^*/(Et)$ is a small dimensionless number as discussed above. These expressions are plotted in Fig. 1b (dashed lines) and match precisely the force-displacement curves measured experimentally (solid lines) for various pressures. The seam-line width e, difficult to measure, has been used as a fitting parameter and yields reasonable values (1.7 mm), close to the estimated measurements.
Linearization of the ratio $FL_0/(l\Delta)$ around the unloaded inflated state ($\beta = \pi$) provides an analytical expression for the stretching modulus perpendicular to the seam direction $Y_\perp$ for infinitesimal deformation.

$$Y_\perp = \frac{2}{\pi} pw^* \tag{15}$$

For small deformations, the effective stretching modulus does not depend on the fabric and is only set by the pressure and the geometry of the air beams. Dividing the force by the pressure results in a collapse of the force vs. strain curves (Fig. 1b inset). Conversely, the stiffness of the structures reaches the stiffness $2Et$ of the pair of sheets for large deformations, as illustrated in Fig. 1b.

Bending. For small bending deformations, pressure does not play any role, since bending conserves volume at the first order bending strain [3]. The bending stiffness $B_\perp$ per unit width of the beam thus corresponds to the bending stiffness of the envelope in the inflated geometry, and reads (we here consider $w^* \simeq w$):

$$B_\perp = Ew^2t/(4\pi) \tag{16}$$

In order to probe this prediction experimentally, slender air beams are subjected to a three-points bending test for various pressures, as shown in Fig. 2(a) and (b). The applied force first displays a linear dependence with the imposed displacement Δz (Fig. 2c), as predicted by classical Euler-Bernoulli beam theory:

$$\Delta z = \frac{FL^3}{48EI} \tag{17}$$

We obtain a fair agreement between the inferred stiffness and its theoretical value $Ew^2t/4\pi$ (Fig. 2d).

Although this linear response is mostly independent of pressure, such an air beam dramatically collapses upon a critical load F_c that strongly depends on pressure, as shown in Fig. 2c. While the profile of the beam follows the classical Euler-Bernoulli description, a sharp king is observed when the force reaches F_c (Fig. 2b). The critical moment per unit width $M_c = \pi F_c L/8w$ is plotted as a function of the pressure for various air beams in Fig. 2e made of different materials and with cross-sections of various widths. The dependence of M_c on p appears to be affine, where the slope varies with the width of the cross-section, while the critical moment at vanishing pressure mainly depends only on the properies of the sheet (Fig. 2e).

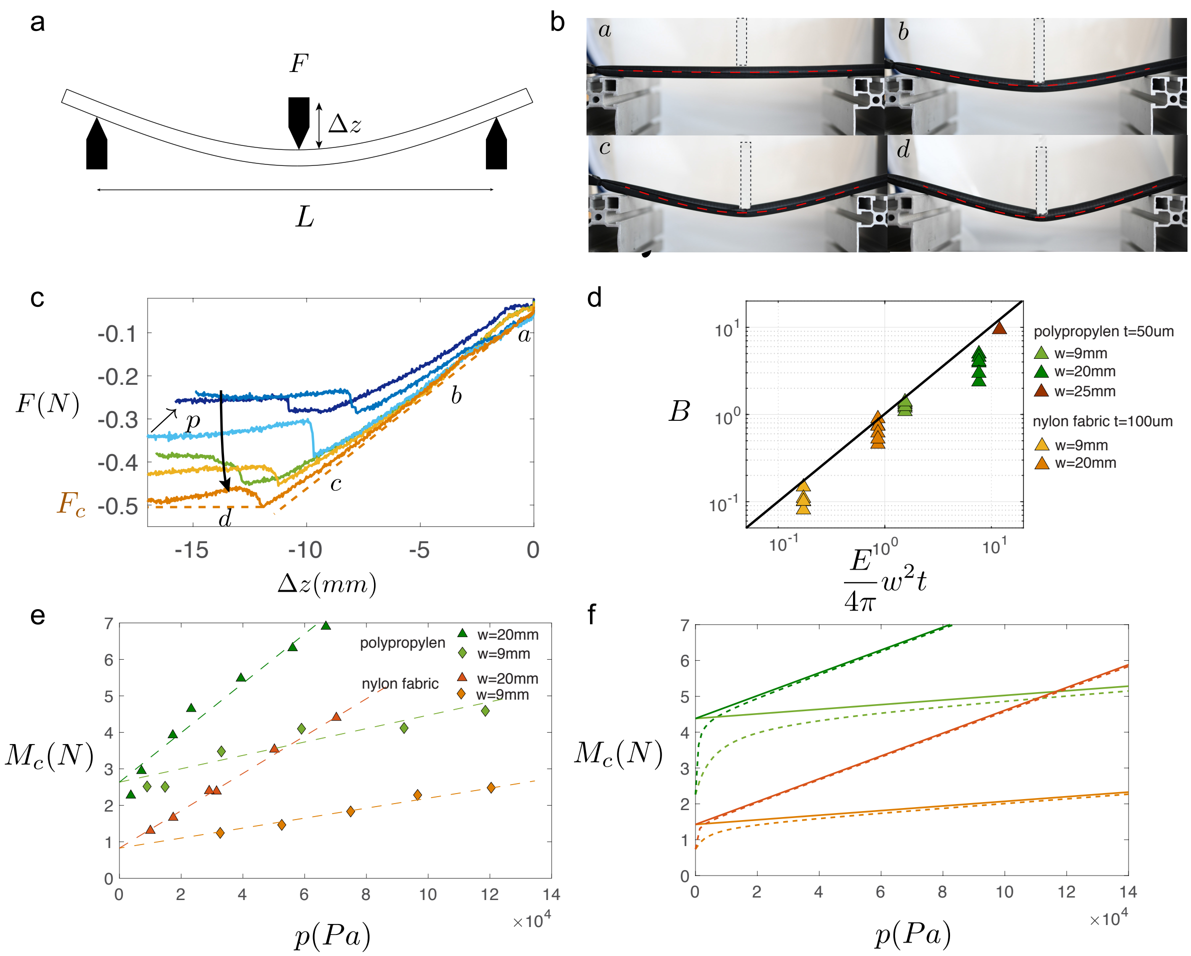

Figure 2: Three-point bending test of a straight inflated beam. (a) Experimental setup. (b) Pictures for various imposed deflections with the superimposed theoretical profile in red dashed lines. The four pictures, labeled by *a, b, c, d*, correspond to different stages of a bending test, the force-displacement curves being shown in (c) for an air beam of deflated width $w = 9\,\mathrm{mm}$ made of a polypropylene sheet of thickness $t = 50\,\mu\mathrm{m}$ and Young's modulus $E = 2.2\,\mathrm{GPa}$. (d) Experimental bending stiffness per unit width B as a function of the theoretical bending stiffness of air beams. Experimental (e) and theoretical (f) critical moments per unit width M_c as a function of pressure accounting for ovalization (dashed lines) or not (solid lines).

Following Calladine [4] and Seide and Weingarten [5], the critical torque M_c for which an air beam collapses is attained when the extreme fibre reaches the critical buckling stress σ_c in the case of uniaxial compression of a cylindrical shell. The critical stress reads $\sigma_c = \pi E t/(\sqrt{3}w)$. In order to reach this critical compressive stress, the imposed moment must additionally overcome the pressure-induced longitudinal tension in the beam, which classically reads $\sigma_p = pw/2\pi t$. Hence the maximum bending moment per unit width that the air beam may sustain reads:

$$
\begin{aligned}
M_c &= \pi w \tfrac{t}{2}[\sigma_c + \sigma_p] &(18)\\
M_c &= \frac{\pi^2 E t^2}{2\sqrt{3}} + \frac{p w^2}{4\pi} &(19)
\end{aligned}
$$

The ovalization of the cross section upon curvature, known as Brazier effect, may be disregarded in these examples, since the applied pressure limits changes of the shape of the cross-section. The theoretical critical momentum with (dashed lines) and without (solid lines) the ovalization of the cross section as a function of the pressure is shown in Fig. 2f. The comparison with experimental data is fairly good.

In a structure constituted by an assembly of straight beams, the bending stiffness $B_\parallel$ along the seams is very weak as it mainly involves bending of the seams, while the inflated region only rotates around these hinges. The bending stiffness of the seams scales classically as Et^3 which is orders of magnitude smaller than the stiffness in the transverse direction (Ew^2t with $w \gg t$). This strong stiffness anisotropy should be avoided to preserve the overall stability and stiffness of the object. Soft structural modes may indeed cause the failure of the structure. Note that this soft mode is possible because the sealed lines are rectilinear, providing the rotation axis. Hence, some variations are needed in the direction of the network of heat-sealed lines, such that a stiff mode will be encountered for any direction and position of bending solicitation.

2 ”Zigzag” Patterns

Stretching. As a force balance approach is not trivial in the case of the stretching of zigzag patterns (Fig. 3a), we propose an energy approach to estimate the stretching rigidity. We restrain ourselves to the “inextensible” regime, for which the total potential energy reads $U = -pV - F\Delta$.

Using the same notations as in the previous section, the expression of the volume of a zigzag structure is:

$$V = \left(1 - \frac{\sin\beta}{\beta}\right)\frac{w^2 n l}{\beta} \tag{20}$$

where n is the number of zigzag segments and l is the length of a single segment. The contraction rate perpendicular to the local seams λ may also be expressed as a function of the spanned angle β (defined in Fig. 1):

$$\lambda = 2\sin(\beta/2)/\beta \tag{21}$$

The displacement Δ along (or perpendicular to) the zigzag direction reads:

$$\Delta = (\lambda_\parallel - \lambda_\parallel^0)L_0 \tag{22}$$

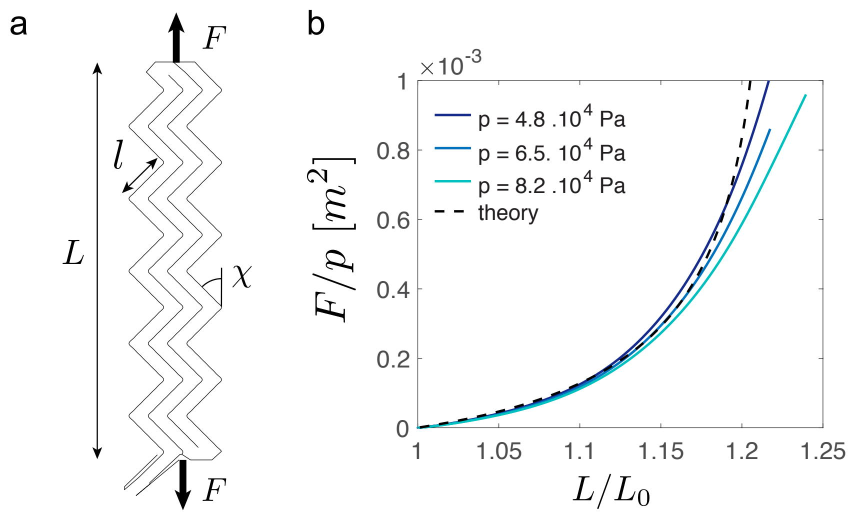

Figure 3: Stretching stiffness of a Zigzag pattern. (a) Sketch of the heat-sealed pattern and of the traction test. (b) Theoretical (dashed line) and experimental (solid lines) force divided by the pressure as a function of the elongation. The seam width of the line e, difficult to measure, has been used as a fitting parameter ($w = 7.2\,\mathrm{mm}$, $n = 33$, $l = 34\,\mathrm{mm}$, $\chi = \pi/4$).

where $\lambda_\parallel = \dfrac{\lambda}{\sqrt{\sin^2\chi + \lambda^2\cos^2\chi}}$, $\lambda_\parallel^0$ is the contraction in the unstretched fully inflated state, that is, for $\beta = \pi$, and L_0 the length of the inflated structure in the rest state. Energy minimization gives us the following expression for the force:

$$F = -p\,\frac{\partial V/\partial\beta}{\partial\Delta/\partial\beta} \tag{23}$$

which becomes, after derivation:

$$F = 2p(w-e)^2 nl\cos(\beta/2)\,\frac{(\tan^2\chi + \mathrm{sinc}^2(\beta/2))^{3/2}}{\beta\tan\chi} \tag{24}$$

The ratio of the experimental force by the applied pressure F/p is plotted as a function of the elongation L/L_0 for various values of the pressure (Fig. 3b). All curves collapse onto one single master curve (at least for small displacements), that is very well fitted by the inextensible theory presented in equation (24), using once again the seam thickness e as a single fitting parameter.

Note that as in the case of miura-ori structures [6], inflated zigzag patterns exhibit an auxetic behaviour: the Poisson ratio is negative around the inflated unstretched state ($\beta = \pi$) and reads:

$$\nu = -\frac{\lambda^2}{\tan^2\chi} \tag{25}$$

This expression is only valid in the inextensible regime, i.e., when χ is sufficiently large.

References

[1] Julien Dervaux and Martine Ben Amar. Morphogenesis of growing soft tissues. Phys. Rev. Lett., 101:068101, Aug 2008.

[2] Emmanuel Siéfert and Mark Warner. Inflationary routes to gaussian curved topography. arXiv preprint arXiv:1912.13425, 2019.

[3] RL Comer and Samuel Levy. Deflections of an inflated circular-cylindrical cantilever beam. AIAA journal, 1(7):1652–1655, 1963.

[4] Chris R Calladine. Theory of shell structures. Cambridge University Press, 1989.

[5] Paul Seide and Victor Weingarten. On the buckling of circular cylindrical shells under pure bending. Journal of Applied Mechanics, 28(1):112–116, 1961.

[6] Mark Schenk and Simon D Guest. Geometry of miura-folded metamaterials. Proceedings of the National Academy of Sciences, 110(9):3276–3281, 2013.